Applied Physics Letters

A perspective on nonlinearities in coherent magnetization dynamics

Cite as: Appl. Phys. Lett. **120**, 050501 (2022); https://doi.org/10.1063/5.0075999
Submitted: 20 October 2021 • Accepted: 19 January 2022 • Published Online: 03 February 2022

Jingwen Li, Chia-Jung Yang, Ritwik Mondal, et al.

Applied Physics Letters PERSPECTIVE scitation.org/journal/apl

A perspective on nonlinearities in coherent magnetization dynamics

Cite as: Appl. Phys. Lett. **120**, 050501 (2022); doi: 10.1063/5.0075999
Submitted: 20 October 2021 · Accepted: 19 January 2022 ·
Published Online: 3 February 2022

Jingwen Li,[1] Chia-Jung Yang,[1] Ritwik Mondal,[2,3,a)] Christian Tzschaschel,[4,a)] and Shovon Pal[5,a)]

AFFILIATIONS

[1]Department of Materials, ETH Zurich, 8093 Zurich, Switzerland
[2]Department of Spintronics and Nanoelectronics, Institute of Physics ASCR, v.v.i, Cukrovarnická 10, Prague 6 162 53, Czech Republic
[3]Department of Physics and Astronomy, Uppsala University, Box-516, 75120 SE Uppsala, Sweden
[4]Department of Chemistry and Chemical Biology, Harvard University, Cambridge, Massachusetts 02138, USA
[5]School of Physical Sciences, National Institute of Science Education and Research, HBNI, Jatni, 752 050 Odisha, India

Note: This paper is part of the APL Special Collection on Ultrafast and Terahertz Spintronics.
[a)]**Authors to whom correspondence should be addressed:** mondal@fzu.cz; ctzschaschel@fas.harvard.edu; and shovon.pal@niser.ac.in

ABSTRACT

The recent thrust in ultrafast magnetization dynamics aims at extending spintronic functionalities to terahertz frequencies. Deterministic manipulation of magnetization at the corresponding ultrashort timescales requires minute control not only over the magnetization itself but also the reservoirs it is interacting with. Although the various intricate couplings between spins, phonons, and electrons—all of which are susceptible to ultrashort laser pulses—lead to many (often nonlinear) coupling routes, magnetization-dynamical nonlinearities have remained largely underexplored. In this Perspective, we highlight recent advances and foresee future developments in the rapidly evolving field of nonlinear magnetization dynamics. Given the elementary character of coherent excitations, we put particular emphasis on their nonlinearities. We briefly review theoretical aspects and assess excitation mechanisms to reach the nonlinear regime of magnetic excitations in a broad class of magnetic materials, such as ferromagnets, antiferromagnets, and ferrimagnets. We present an overview of the groundbreaking experiments that showcase the unique insights provided by magnetic nonlinearities. We conclude by discussing open challenges and opportunities that underpin the potential of nonlinear magnetization dynamics for the advancement of spintronics and cavity quantum electrodynamics with spin waves at terahertz frequencies.

I. INTRODUCTION

The vast majority of data is currently stored in magnetic memories, where opposite magnetic states are used to encode logical "0" and "1." Both magnetic states are stable energy minima of the magnetization, i.e., close to the ground state, the energy increases parabolically with respect to small perturbations of the magnetization. The magnetization dynamics in a static parabolic potential are exactly solvable and resemble the linear dynamics of a simple harmonic oscillator.[1–4] In particular, the deviation of the magnetization from the ground state increases linearly with the driving excitation.

Interestingly, as an immediate consequence of the presence of at least two stable states, the energy landscape *must* deviate from the parabolic behavior for sufficiently large perturbations.[5] These deviations form the foundations of nonlinear magnetization dynamics. In particular, switching of magnetization, e.g., in a magnetic memory, is a highly nonlinear process, where even small changes in the applied magnetic field can result in large changes to the magnetization. Understanding nonlinear magnetization dynamics, thus, directly advances and accelerates the development of ways for manipulating magnetization enabling a higher data density, faster processing speed, and better energy efficiency of next-generation information technologies.

The conventional way to alter magnetization is to apply an external magnetic field, the speed of which is in the nanosecond timescales,[6–8] limited by the speed of relativistic electron switch.[9,10] In contrast, optical fields can manipulate magnetization on much faster timescales ranging from picosecond[11] and sub-picosecond[12] to sub-femtosecond.[13] Scrupulous observations in the attosecond timescales indicate that the optically induced transfer of momentum is in

harmony with the light-field-driven relocation of coherent charge density.[13] Such ultrafast magnetization dynamics convey a multitude of information on the magnetic materials, such as anisotropy energies,[14,15] the strength of the exchange couplings,[16] dipole fields,[17] and the existence of magnetic phase transitions.[10,18] In most experiments, a linearly polarized femtosecond optical pulse leads to a rapid increase in the temperature as a result of optical absorption, limiting potential applications. Circularly polarized femtosecond laser pulses, however, can be used for non-thermal excitation and coherent control of the magnetization dynamics via an inverse Faraday effect (IFE).[19–21] Very recently, within the past decade, such manipulation of magnetic order is achieved and experimentally demonstrated by using intense single-cycle terahertz (THz) pulses.[22–24]

Unlike femtosecond optical pulses, intense THz pulses interact with the spins on the intrinsic energy scales of magnetic excitations through the Zeeman-torque that is caused by the magnetic field component of the THz pulse. This is a rather direct, efficient, and a faster means of controlling the magnetization dynamics. While the excitation through Zeeman-torque can still be described within the linear excitation regime, there are several ways for the THz pulses to drive such excitation beyond the linear regime,[14,25] such as by using THz driving fields amplitudes as high as tens of Tesla or more where nonlinear coupling routes are mostly involved (see Fig. 1 for a schematic overview), such as electric dipole-mediated nonlinear THz-spin coupling, spin-phonon equilibration, nonlinear damping, inertia-driven spin nutations, the electric-field-induced anisotropy changes, effective magnetic field from rotations and displacements of crystal-field atoms, or via magnetoelectric coupling in multiferroic materials.

In this Perspective, we begin with a simple introductory-like discussion on the magnetization dynamics using the established notions of Landau–Lifshitz–Gilbert (LLG) formalism to get our readers into the stage of the current discussion on the nonlinear magnetization dynamics in a broad class of magnetic materials that involve ferromagnetic, antiferromagnets, and ferrimagnets. From here, we will elaborate on the nonlinear means of manipulating the magnetization at ultrafast timescales. We will also elaborate on driving the magnetization precession with intense THz light in a manner that it generates nonlinear frequency components. On the way, we will revisit the current developments of THz spintronic applications and give a perspective on experiments, theoretical models, and future developments that we foresee will happen in the field of ultrafast manipulation of magnetization in ferro-, ferri-, and antiferromagnets. The ultimate speed is, however, an ever-evolving research direction that bears significant potentials toward fast and energy-efficient data processing and storage applications.

II. MAGNETIZATION DYNAMICS

The THz magnetization dynamics that form the focus of the present perspective occur primarily in ferrimagnets and antiferromagnets, i.e., magnetic systems with several magnetic sublattices, while in ferromagnets (with a single magnetic lattice), the magnetization precession occurs at GHz frequencies. The coherent dynamics of the

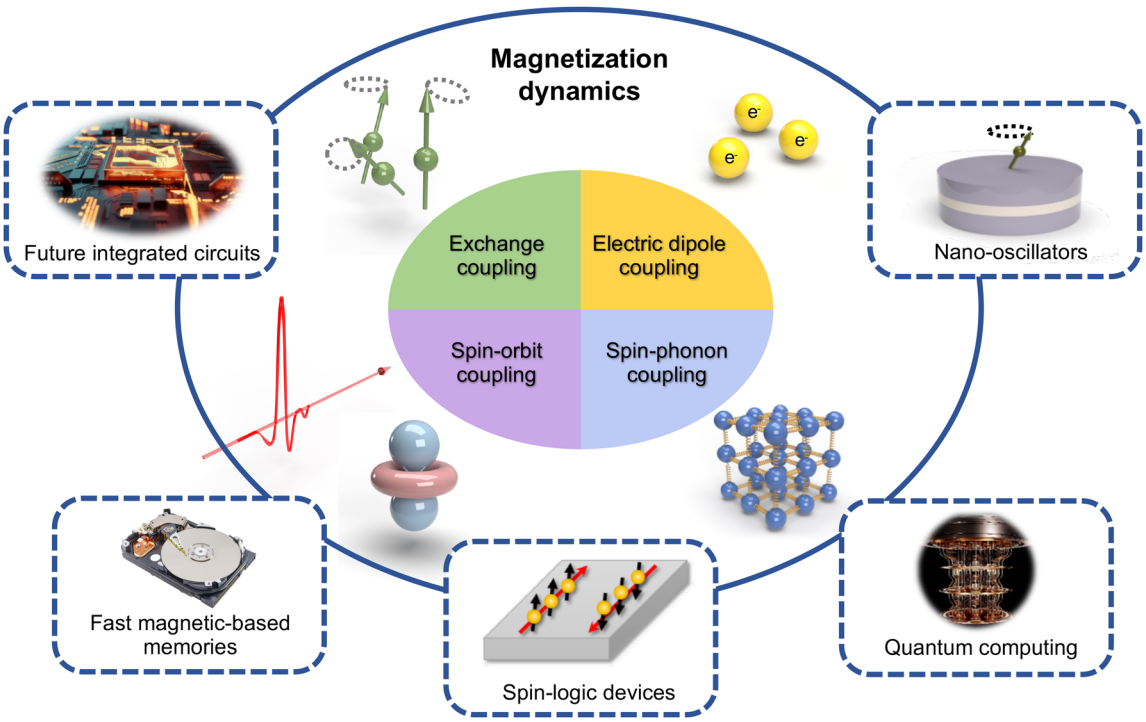

FIG. 1. A conceptual overview on coherent magnetization dynamics. The inner circle shows the several important effects that contribute to the light-induced magnetization dynamics and their corresponding energy reservoirs. The outreach of fundamental effects emerging from these reservoirs, such as inertial torque, field-derivative torque, exchange torque, and the associated dynamics hinges the outer circle, concomitantly paving the way toward several future applications of coherent magnetization dynamics. Pictures within future integrated circuits (© J. Thew), fast magnetic-based memories (© Dsom), and quantum computing (© B. Wróblewski) are reprinted with permission from Adobe Stock—stock.adobe.com. Copyright 2021 Adobe.

magnetization $\mathbf{M}_\alpha$ of the α-th sublattice with magnitude $M_{S,\alpha}$ are commonly described by the LLG equation,

$$\dot{\mathbf{M}}_\alpha = -\frac{\gamma_\alpha}{1+\alpha_\alpha^2}\mathbf{M}_\alpha \times \mathbf{B}_\alpha^{\text{eff}} - \frac{\gamma_\alpha \alpha_\alpha}{(1+\alpha_\alpha^2)M_{S,\alpha}}\mathbf{M}_\alpha \times \left(\mathbf{M}_\alpha \times \mathbf{B}_\alpha^{\text{eff}}\right), \quad (1)$$

with the, in general, sublattice-dependent gyromagnetic ratios γ_α as well as Gilbert damping parameters α_α, and an effective magnetic field $\mathbf{B}_\alpha^{\text{eff}}$ acting on the magnetization. In general, for a magnetization that is described by a free energy density $\mathcal{F}$, the effective magnetic field is defined as $\mathbf{B}_\alpha^{\text{eff}} = -\delta\mathcal{F}/\delta\mathbf{M}_\alpha$. The free energy density $\mathcal{F} = \sum_\alpha \mathcal{F}_\alpha + \sum_{\alpha\beta}\mathcal{F}_{\alpha\beta}$ is in general composed of terms $\mathcal{F}_\alpha$ that describe the free energy of individual sublattices as well as terms $\mathcal{F}_{\alpha\beta}$ that relate to the exchange coupling between different magnetic sublattices. In the following, for equations referring to any sublattice, we will omit the subscript α. We denote the sublattice magnetization by $\mathbf{M}$ and the effective magnetic field acting on that sublattice by $\mathbf{B}$. The two terms of Eq. (1) are usually referred to as the field torque and the damping torque. They induce a precessional motion around the effective magnetic field and a relaxation toward the field direction, respectively. In equilibrium, $\mathbf{B}^{\text{eff}}$ is either parallel to $\mathbf{M}$ or vanishes. Out of equilibrium, typical timescales of precessional magnetization dynamics are given by $|\gamma\mathbf{B}^{\text{eff}}|^{-1}$, which covers from several nanoseconds for a ferromagnetic magnetization precession in a weak external field to sub-picoseconds for antiferromagnetic magnetization dynamics driven by the strong exchange fields between neighboring spins.

Magnetization dynamics can be induced by perturbing the effective magnetic field, i.e., $\mathbf{B}^{\text{eff}} = \mathbf{B}_0^{\text{eff}} + \Delta\mathbf{B}^{\text{eff}}$. Suppose the magnetization is initially static i.e., $\dot{\mathbf{M}}(t=-\infty) = 0$. Magnetization dynamics describe a deviation of the magnetization from the initial state, i.e., $\Delta\mathbf{M}(t) = \mathbf{M}(t) - \mathbf{M}(t=-\infty)$. In analogy to classical nonlinear dynamics,[26] we define nonlinear magnetization dynamics in the following way: suppose that $\Delta\mathbf{M}_\text{A}(t)$ and $\Delta\mathbf{M}_\text{B}(t)$ describe the time-evolution of the magnetization in response to perturbations A and B of the effective magnetic field $\Delta\mathbf{B}_\text{A}^{\text{eff}}$ and $\Delta\mathbf{B}_\text{B}^{\text{eff}}$ according to Eq. (1). We refer to the magnetization dynamics as *linear* if, and only if,[27]

$$\Delta\mathbf{M}_\text{AB}(t) = \Delta\mathbf{M}_\text{A}(t) + \Delta\mathbf{M}_\text{B}(t) \quad (2)$$

describes the time evolution of the magnetization $\mathbf{M}$ in response to the perturbation $\Delta\mathbf{B}_\text{A}^{\text{eff}} + \Delta\mathbf{B}_\text{B}^{\text{eff}}$. Consequently, we define magnetization dynamical nonlinearities as

$$\mathbf{M}_\text{NL}(t) = \Delta\mathbf{M}_\text{AB}(t) - \Delta\mathbf{M}_\text{A}(t) - \Delta\mathbf{M}_\text{B}(t). \quad (3)$$

Although other definitions of magnetization dynamical nonlinearities may be more practical in certain experimental settings,[15,28] Eq. (3) would always be capable of capturing the nonlinear component of the magnetization dynamics and, therefore, constitutes a general definition of magnetization dynamical nonlinearities. Equation (3) provides not only a general formalism to identify the presence of magnetic nonlinearities irrespective of their microscopic origin, but also an explicit guidance on how to detect magnetic nonlinearities experimentally. In fact, Eq. (3) forms the widely established basis for the experimental investigation of nonlinear magnetization dynamics in the context of 2D-THz spectroscopy.[29–36] Such experiments are the focus of Sec. IV in this Perspective.

The efficient excitation of magnetization dynamics requires a variation of $\mathbf{B}^{\text{eff}}$ on the intrinsic timescales of the magnetic system. Such modulation can be either a *resonant*, i.e., periodic with the intrinsic magnetization precession frequency, or *impulsive*, i.e., an abrupt change in a timescale much shorter than the precession frequency. The latter usually rely on ultrashort laser pulses, which trigger sudden changes in $\mathbf{B}^{\text{eff}}$, e.g., due to magneto-optical coupling effects. To illustrate the origin of the laser-induced change in $\mathbf{B}^{\text{eff}}$, we consider the following generic free energy density for a particular magnetic sublattice,

$$\mathcal{F}_\alpha = D_{ij}M_iM_j - B_iM_i + \underbrace{\left(\chi_{kl}^{(0)} + ik_{ikl}M_i + g_{ijkl}M_iM_j\right)}_{\text{dielectric susceptibility}} E_kE_l^* + \cdots. \quad (4)$$

While the first two terms give the single-ion anisotropy with an anisotropy tensor D_{ij} and the Zeeman energy in an external magnetic field $\mathbf{B}$, respectively, it is the last term that describes the interaction between the material and the electric field of the laser pulse. Note that the free energy expression in Eq. (4) contains the contributions from one sublattice. For multisublattice magnets, such as antiferromagnets, similar energy contributions have to be taken into account for other sublattices as well. We expand the dielectric susceptibility tensor up to second order in the magnetization. The zeroth-order term $\chi^{(0)}$ describes the interaction in the paramagnetic phase. The magneto-optical coupling tensors k_{ijk} and g_{ijkl} give rise to the IFE[37] and the inverse Cotton-Mouton effect (ICME),[38] respectively. A simple rearrangement of the terms in the free energy reveals the nature of the inverse magneto-optical effects,

$$\mathcal{F}_\alpha = \left(D_{ij} + g_{ijkl}E_kE_l^*\right)M_iM_j - \left(B_i - ik_{ikl}E_kE_l^*\right)M_i + \chi_{kl}^{(0)}E_kE_l^* + \cdots. \quad (5)$$

The ICME describes an optically induced change of magnetic anisotropy, whereas the laser pulse acts as a magnetic field via the IFE. Both mechanisms can give rise to a non-thermal instantaneous change in $\mathbf{B}^{\text{eff}}$. As $\mathbf{B}^{\text{eff}}$ is defined for each sublattice individually, ultrafast changes of $\mathbf{B}^{\text{eff}}$ can even be used to induce magnetization dynamics in fully compensated antiferromagnets.[39,40] For ideal impulsive excitations, the time-dependent change in $\mathbf{B}^{\text{eff}}$ can be approximated by a δ-function, i.e., $\Delta\mathbf{B}^{\text{eff}} = \mathbf{B}_{\text{opt}}^{\text{eff}}\tau\delta(t)$, where τ corresponds to the laser pulse duration and $\mathbf{B}_{\text{opt}}^{\text{eff}}$ is the optically induced change in $\mathbf{B}^{\text{eff}}$ [see Fig. 2(a) (left)]. Integrating the LLG equation, the field torque causes an instantaneous rotation of $\mathbf{M}$ around the direction of $\mathbf{B}_{\text{opt}}^{\text{eff}}$ by an angle of $\phi \sim \gamma\mathbf{B}_{\text{opt}}^{\text{eff}}\tau$, whereas the damping torque aligns the magnetization with $\mathbf{B}_{\text{opt}}^{\text{eff}}$ by $\alpha\phi$. While the field-torque contribution is frequently considered for optically induced coherent magnetization dynamics, the damping-torque contribution can often be neglected in weakly damped ferromagnets ($\alpha \ll 1$). In antiferromagnets, however, the damping-torque can overcome the antiferromagnetic exchange interaction and induce a net magnetization. This process was recently found to be capable of inducing spin precessions with amplitudes comparable to the field-torque contribution despite $\alpha \ll 1$.[41]

Although optically induced spin deflection angles of up to 1° have been observed experimentally,[43] questions remain on how to enhance such impulsive spin excitations to enable not only the observation of magnetization dynamical nonlinearities, but also magnetic switching. A key bottleneck of impulsive excitation mechanisms arises

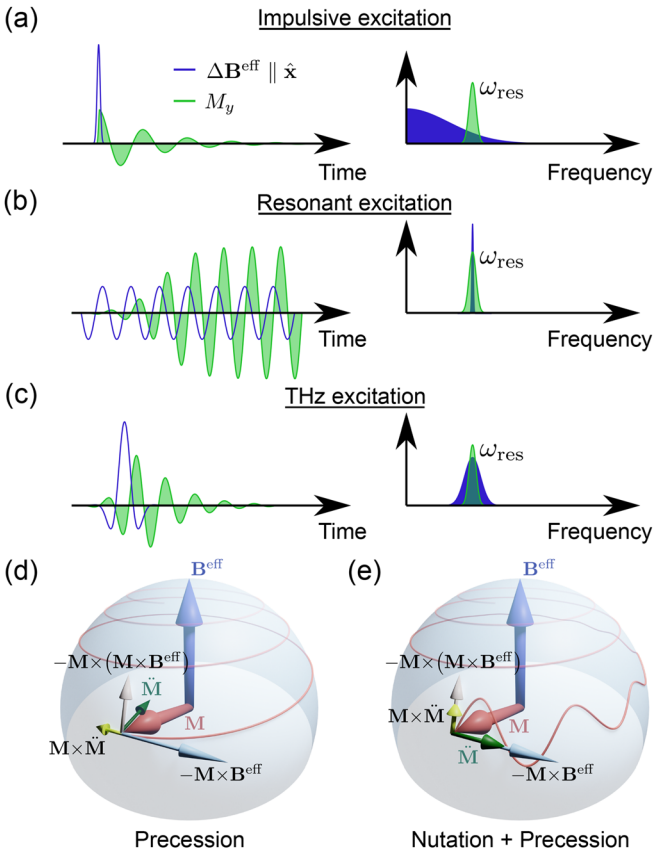

FIG. 2. Excitation pathways and precession schemes. (a) Impulsive excitations are characterized by a large, but temporally short change of $\mathbf{B}^{\text{eff}}$. A poor spectral overlap limits achievable excitation amplitudes. (b) Resonant excitations can induce large angle spin precessions, but suffer from poor temporal resolution. (c) THz excitations combine the best of both worlds. A good spectral overlap enables efficient spin excitation on the timescale of the precession period. (d) A schematic of the magnetization precession. For a steadily precessing spin, the inertial torque points opposite to the field torque resulting in a reduction of the precession frequency.[42] (e) A schematic of the spin nutation. An abruptly activated $\mathbf{B}^{\text{eff}}$ accelerates the originally static magnetization [$\dot{\mathbf{M}}(t=0)=0$] in the direction of the precession. The corresponding inertial torque induces a nutation on top of the precession.

from the fundamentally limited spectral overlap between the exciting optomagnetic field and the spin precession frequency [see Fig. 2(a) (right)]. Resonant excitation, however, circumvents this limitation at the expense of temporal resolution by periodically driving the magnetic order over several periods of the magnon resonance [shown in Figs. 2(b)]. Ferromagnetic resonance (FMR) spectroscopy constitutes the ultralong limit of resonant excitations. Indeed, recent studies observed a deeply nonlinear regime of magnetization dynamics in ferromagnetic nanomagnets using resonant quasi-continuous-wave microwave excitation.[42] Magnetization precession angles of 84° induced a significant time-periodic modulation of the demagnetizing field giving rise to nutation waves—a nonlinear magnetization precession that is absent for small-angle excitations. On the one hand, such observations showcase the possibilities enabled by resonant spin excitations. On the other hand, resonant excitations require a source that can provide a magnetic field with a frequency matching of the magnetic resonance frequency. While sources in the low-GHz regime are readily available enabling the investigation of ferromagnets, such a requirement hampers the investigation of ferrimagnets and antiferromagnets, where typical resonance frequencies are in the high GHz to a few THz regime. The recent use of frequency extenders enables (anti-) ferromagnetic resonance spectroscopy up to ∼1 THz, thus providing a promising tool for the future investigation of nonlinear magnetization dynamics in antiferromagnets.[44,45]

Intense few-cycle THz pulses combine the best of both worlds. Tuned to the magnetic resonance frequency, they provide a good spectral overlap enabling efficient resonant spin excitations [see Figs. 2(c)]. At the same time, few-cycle THz pulses provide sub-picosecond temporal resolution allowing for the investigation of ultrafast coherent magnetization dynamics. Indeed, single-cycle THz pulses with peak magnetic fields of 0.4 T were found to induce a spin deflection of 2° in NiO, which was sufficient for the observation of magnetization nonlinearities.[15] Given the tremendous success and importance of THz radiation for the excitation of nonlinear magnetization dynamics, we will provide a more detailed review and perspective on the THz nonlinearities using two intense, time-delayed THz pulses in Sec. IV.

Despite its success in explaining a wide range of magnetization dynamical processes and nonlinearities, it was recently realized that the original LLG equation as stated in Eq. (1) does not account for all relativistic and quantum effects that can cause additional torques, in particular, at ultrafast timescales.[46,47] This triggered a flurry of phenomenological extensions based on the original LLG equations. From the point of view of ultrafast magnetization dynamics, two extensions are particularly noteworthy. On the one hand, in addition to field torque and damping torque, there are *inertial torques* of the form[48–53]

$$T_{\text{inertial}} = \frac{\eta}{M_S}(\mathbf{M}\times\ddot{\mathbf{M}}), \tag{6}$$

where the relaxation time η defines a moment of inertia for the magnetization $\mathbf{M}$. From a simple dimensional analysis, it is evident that while the Gilbert damping is dimensionless, the moment of inertia η has the dimension of time. On the other hand, there are *relativistic field-derivative torques* (rFDT), which are based on a renormalization of the effective magnetic field in the LLG equation as[46,54]

$$\mathbf{B}^{\text{eff}} \rightarrow \mathbf{B}^{\text{eff}} - \frac{\alpha V_{\text{uc}}}{\gamma M_S}\dot{\mathbf{H}}(t). \tag{7}$$

Here, V_{uc} is the volume of the unit cell and $\mathbf{H}(t)$ is the time-dependent applied Zeeman field. We will now discuss the implications of these extensions to the conventional LLG equation in detail.

A. Inertial dynamics

The initial formulation of the LLG equation assumed a strict relation between the angular momentum $\mathbf{L}$ of an electron and its magnetic moment $\boldsymbol{\mu} = \gamma\mathbf{L}$ consistent with experimental observations at the time.[49] Recent experiments, however, revealed that this relationship can be violated at ultrafast timescales, which necessitated a more general description including a moment of inertia of the magnetic moment.[55] Although the microscopic origin of spin inertia (also including the thermal agitation) has been debated in the literature,[53,56–60] an inclusion of the inertial torque into the LLG equation could explain the experimental observations. Moreover, the inertial torque has intriguing implications on the precessional and the ultrafast

magnetization dynamics that are experimentally under-explored so far.

Let us briefly consider a conventional magnetization precession [shown in Fig. 2(d)]. In the absence of damping, the magnetic acceleration $\ddot{\mathbf{M}}$ is always perpendicular to the precessional motion. Therefore, the inertial torque T_{inertial} points opposite to the field-like torque in the LLG equation. As such, it reduces the precession frequency. While the $\ddot{\mathbf{M}}$ is proportional to the square of the precession frequency and hence the magnetic field, the field-like torque driving the precession, in contrast, is proportional to $\mathbf{B}^{\text{eff}}$, leading to an intrinsic nonlinear competition between the inertial torque and the field-like torque. The effect of inertial torque T_{inertial} is even more striking at ultrafast timescales. Figure 2(d) illustrates the situation for an initially steady magnetization vector $\mathbf{M}(0)$ [$\dot{\mathbf{M}}(0) = 0$]. An abruptly changing effective magnetic field causes a magnetic acceleration that is tangential to the precessional motion. In this case, the inertial torque induces a nutation of the magnetization, as shown in the schematic of Fig. 2(e).

In experiments, the magnetic nutation introduces an additional resonance peak in the FMR spectrum.[2,61] While the precessional resonance peak occurs in the GHz regime for ferromagnets in the presence of reasonable magnetic fields, the nutation peak occurs in the THz regime.[55,62,63] Even though the characteristic timescales of the spin nutation, η, has been predicted within the range of 1–100 fs,[49,56] the experimental findings show that $\eta \sim 300$ fs in CoFeB.[55] The additional nutation resonance peak appears at a frequency $\nu_{\text{nutation}} \sim 1/\eta$, that is higher than the FMR frequency.[2,64]

Beyond the ferromagnetic magnetization dynamics, a linear response theory of inertial magnetization dynamics applied to antiferromagnets shows much promising significance of spin nutation. The reduction of antiferromagnetic precession resonance frequencies is stronger than that of the ferromagnets due to the generally higher precession frequencies in antiferromagnets. In fact, for antiferromagnets, the precession and nutation resonance frequencies both lie in the THz regime. This offers an advantage of detecting nutation dynamics in two-sublattice antiferromagnets over ferromagnets. Moreover, the nutation resonance peak in antiferromagnet is exchange-enhanced.[65,66] The latter implies that antiferromagnetic nutation resonance should be better detected in the experiments.[65,67] Exploiting the nutation might enable advanced pathways for magnetization switching. In this highly nonlinear regime, both the precession and nutation frequency depend on the magnetization direction. Exploration of such nonlinear nutation dynamics opens a completely different field within the realm of nonlinear magnetization dynamics.

We note that in antiferromagnets, the intrinsic inertial dynamics is also caused by the exchange interaction, where the exchange energies, created by the tilting of spin moments, are dynamically transformed to the anisotropy energies.[68] Such inertial dynamics, however, do not lead to the spin nutation in antiferromagnets as we have discussed here.

B. Field-derivative dynamics

The rFDT provides a nonlinear effect in the large damping limit. Such rFDT arises due to the fact that *not only* the magnetic field from the laser pulse couples to the spins, *but also* the time-derivative of the magnetic field couples to the spins. Such differentiation additionally introduces a 90° phase shift in the effective magnetic field, and, thus, the same phase shift is also expected in the coherent magnon excitation as well. The explicit LLG equation with the rFDT reads as[69]

$$\dot{\mathbf{m}}(t) = -\frac{\gamma}{(1+\alpha^2)}\mathbf{m}\times\left(\mathbf{B}^{\text{eff}} - \frac{\alpha V_{\text{uc}}}{\gamma M_{\text{S}}}\dot{\mathbf{H}}(t)\right) - \frac{\gamma\alpha}{(1+\alpha^2)}\mathbf{m}\times\left[\mathbf{m}\times\left(\mathbf{B}^{\text{eff}} - \frac{\alpha V_{\text{uc}}}{\gamma M_{\text{S}}}\dot{\mathbf{H}}(t)\right)\right], \quad (8)$$

where $\mathbf{m} = \mathbf{M}/M_{\text{S}}$. The sublattice index α has been omitted here as discussed earlier. Note that both field-like and damping-like contributions of the rFDT are present in Eq. (8). While the field-like rFDT scales with the damping parameter α, the damping-like contribution scales with α^2. At the low damping limit, $\alpha \ll 1$, one can ignore the damping-like rFDT contributions, keeping only the field-like rFDT terms that are linear in damping. As soon as the damping becomes larger, both of these rFDT terms contribute, leading to a nonlinear magnetization response. Such effects have been recently investigated in ferrimagnetic iron garnet $Tm_3Fe_5O_{12}$ in the low damping limit.[70] It is, thus, reasonable to foresee experimental verification of rFDT in the nonlinear (large damping) regime as well in the near future.

III. PHONON-ASSISTED NONLINEARITIES

Intense light pulses in the THz frequencies are also capable of driving ionic motions via collective excitations of one or more lattice (phonon) modes. Consider, for example the case of $ErFeO_3$, which upon excitation, the oxygen ions perform rotational motion as depicted in Fig. 3(a). Such motions would modify the crystal field[73] felt by the ions that carry spins in material (in the present, Fe^{3+} at the center of the octahedron). As a result of this, the ground state $t_{2g}^3 e_g^2$ electronic wavefunction at each Fe^{3+} ion mixes with the excited-state orbitals. The moving ions, thereby, perturb the angular momentum of the electronic ground state behaving as an effective magnetic field given by $\partial H_{\text{eff}}/\partial M_{\text{c}} = i\alpha_{\text{abc}} Q_{\text{ua}} Q_{\text{ub}}^*$ that concomitantly trigger the magnetic excitations.[71] Here, a, b, and c are the crystallographic axes, α_{abc} is the magneto-elastic susceptibility, Q_{ua} and Q_{ub} are the phonon eigenvectors corresponding to the infrared active in-plane phonons in $ErFeO_3$, and M_{c} is the static magnetization. Upon direct lattice excitation with an intense 20 THz pulse, the polarization of the 800 nm-probe oscillates as a function of pump-probe delay time, see Fig. 3(c). The coherent oscillations, thereby, reveal a number of Raman-active modes [shown in Fig. 3(d)], such as the 3.36 THz A_{1g}+B_{1g} phonon and the 4.85 THz B_{1g} phonon [within the fast oscillations plotted as gray in Fig. 3(c)]. In addition, the excitation of a coherent quasi-antiferromagnetic mode at 0.75 THz was also observed [shown as red oscillations in Fig. 3(c)]. With the ultrafast intense THz excitation, a pair of phonon-polariton response is initiated within the material. This pair propagates within the material with a very high speed of 0.4×10^8 m/s and carries an effective magnetic field of 36 mT, which then acts as a source for the excitation of the spin waves.[71] The effective magnetic field can be made larger, either by increasing the incident THz field strength or by optimizing the choice of phonon modes with a proper phase matching condition via pulse shaping.

Phonon-induced magnetism has also been realized in yet another rare-earth orthoferrites—$DyFeO_3$.[72] The material displays strong exchange interactions between the spins of the transition metal ion and the rare earth ion along with a strong orbital momentum of the rare-earth ion. This leads to a first-order spin-reorientation phase transition accompanied by a change in the magnetic symmetry from

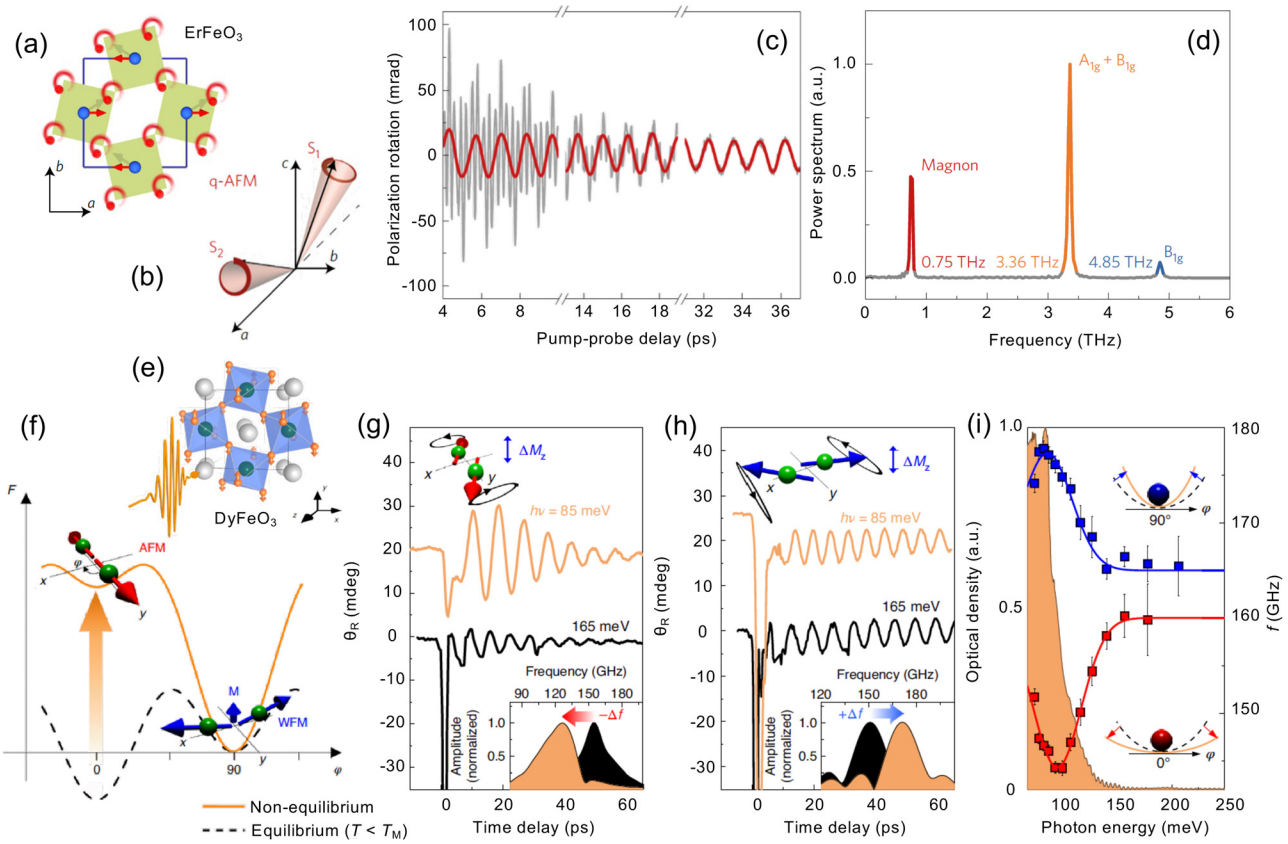

FIG. 3. Phonon-assisted nonlinearities. (a) The ionic motion that leads to an elliptically polarized phononic field in an orthorhombically distorted perovskite structure of $ErFeO_3$. (b) Schematic of the spin motion corresponding to S_1 and S_2 for the 0.75 THz quasi-antiferromagnetic mode. (c) 20 THz-Pump-induced 800 nm-probe polarization changes in $ErFeO_3$ at 100 K. By applying a 1.5 THz-cutoff low-pass filter, the fast oscillations (gray) can be filtered out, thereby revealing the 0.75 THz quasi-antiferromagnetic magnon mode (red). (d) Spectrum of the oscillatory signal in (c) that shows the 0.75 THz quasi-antiferromagnetic magnon, the 3.36 THz Raman phonon with $A_{1g} + B_{1g}$ symmetry and the 4.85 THz Raman phonon with B_{1g} symmetry. (e) Excitation of the B_u phonon mode, where the orange arrows indicate the atomic motion of the oxygen ions in $DyFeO_3$. (f) The magnetic potential F as a function of the angle that the spins form with the y-axis before (dashed black line) and after (orange line) phonon excitation. The spin configurations corresponding to the antiferromagnetic and weakly ferromagnetic phases are indicated by the red and the blue arrows, respectively. The destabilization of the antiferromagnetic ground state is indicated by the orange arrow. Time-resolved Faraday rotation of the probe polarization after light excitation with photon energies of 85 meV (orange traces) and 165 meV (black traces, control experiment) performed in the (g) antiferromagnetic and (h) weak-ferromagnetic phases. (i) The central frequency of the excited soft mode as a function of the photon energy of the pump pulse in the antiferromagnetic (red) and the weak-ferromagnetic (blue) phase. Reprinted with permission from Nova *et al.*, Nat. Phys. **13**, 132 (2017). Copyright 2017 Springer Nature Limited. Reprinted with permission from Afanasiev *et al.*, Nat. Mater. **20**, 607 (2021) Copyright 2021 Springer Nature Limited.[71,72]

the antiferromagnetic phase to the weakly ferromagnetic phase.[74] By using a sub-picosecond intense THz pulse that is in resonance with a phonon mode [as shown in Fig. 3(e)], a coherent spin-reorientation can be driven, concomitantly developing a long-living weak ferromagnetic order. Figure 3(f) shows schematically that the light-induced oscillations of atoms can be driven far from their equilibrium positions, altering the strength of the Fe–Dy exchange interaction[75,76] and, hence, realizing lattice control of the spin arrangement on an ultrafast timescale. When pumped in resonance with the lattice vibrational mode at 20.56 THz (= 85 meV), the light-induced dynamics of the Faraday signal shows coherent oscillations in both the antiferromagnetic and weak-ferromagnetic phases, corresponding to spin precession around their respective equilibrium, see Figs. 3(g)–3(h). Upon Fourier transforming these oscillations, it was found that the spin precession is shifted oppositely for the two phases [see the insets of Figs. 3(g)–3(h)]. While the red shift indicates a flattening of the potential energy in the vicinity of the antiferromagnetic minimum, the blue shift results from an increased curvature of the potential and enhanced phase stability in the vicinity of the weak-ferromagnetic minimum,[72] as shown in Fig. 3(i).

Resonant excitation at ultrafast timescales can in fact be achieved for both longitudinal and transverse optical phonon modes. Recent experiments show that while excitation of transverse mode only results in a thermal demagnetization, the longitudinal modes in the magnetic garnet film reveal a peculiar magneto-elastic switching mechanism.[77] The achieved switching further dictates that the nonlinear phonon-assisted strain assures that the strain pulse generated by the phonon mode is shorter than the magnetization precession period. Resonant pumping of infrared-active phonons with intense ultrashort multi-THz pulses, in addition, reshapes the magnetic potentials to initiate

ultrafast magnetization dynamics and ultimately coherent magnetic phase transitions.[77]

Phono-magnetic effects[75,78] clearly provide a promising toolkit to control magnetization dynamics at fast timescales. The effective magnetic fields that are provided by the phonon analogs of the IFE and ICME on the spins are either comparable or potentially even larger than the opto-magnetic fields.[75,79–81] The phonon-modulated exchange interactions occur on a picosecond timescale, during which there is a redistribution of energy among the phonons and the spins. The angular momentum, however, is only transferred between the spins. The flow of the angular momentum can occur via a direct exchange torque or through the transfer of the spin-polarized electrons.[82] Such transfer of the angular momentum between the spin sublattices plays a determinant role in the switching of magnetization when excitation by a femtosecond laser pulse.[77]

IV. HIGHER-ORDER MAGNON MODES

Magnons are referred to as collective spin waves associated with the spin dynamics in a magnetic material. Experimentally, they reveal themselves through free induction decay-like signals when excited by continuous or pulsed THz fields. A good example is the excitation of spins in antiferromagnetic NiO with the help of THz pulses via Zeeman-torque.[84] Note that the observation in Ref. 70 is still in the linear excitation regime. It is, however, possible to take such a magnon mode to the nonlinear regime, i.e., beyond the perturbative regime, once the driving THz field approaches amplitudes of 10 T or more. Another example of a typical antiferromagnetic magnon [a schematic of the mode is shown in Fig. 4(a)] signals from single crystals of $YFeO_3$ in time and frequency domains are shown in Figs. 4(b) and 4(c), respectively. The THz-active magnon modes can be interpreted as cooperative motions of two sublattices with different spin structures. The higher-order (nonlinear) magnon signals provide extensive insights on the microscopic picture of the spin interactions and hence the magnetization dynamics. In 2D nonlinear THz spectroscopy,[34,36,85–87] such nonlinear signals can be accessed by using a pair of time-delayed intense THz pulses, A and B, which is similar to the conventional 2D magnetic resonance spectroscopy. The nonlinear THz field $\mathbf{B}_{\mathrm{NL}}(t_s, \tau_{\mathrm{delay}})$ [the magenta curve in Fig. 4(e)] is obtained by using the relation $\mathbf{B}_{\mathrm{NL}}(t_s, \tau_{\mathrm{delay}}) = \mathbf{B}_{\mathrm{AB}}(t_s, \tau_{\mathrm{delay}}) - \mathbf{B}_{\mathrm{A}}(t_s, \tau_{\mathrm{delay}}) - \mathbf{B}_{\mathrm{B}}(t_s)$, where τ_{delay} is the delay time and t_s is the sampling time of the THz pulses. $\mathbf{B}_{\mathrm{A}}$ ($\mathbf{B}_{\mathrm{B}}$) are the transmitted THz magnetic fields measured with only pulse A (B), see the blue (red) curves in Fig. 4(d). $\mathbf{B}_{\mathrm{AB}}$ is the transmitted THz magnetic field when both pulses A and B have interacted with the sample [see the black curve in Fig. 4(e)].

The observed nonlinearities of purely magnetic origin can be understood in terms of multiple field-spin interactions. These interactions lead to second-order or third-order nonlinear magnon signals, for example, magnon spin echoes and 2-quantum signals. Lu *et al.* demonstrated that the presence of such signals in single crystals of $YFeO_3$ reveals pairwise correlations between the magnons at the Brillouin zone center.[33] Similar preliminary investigations also show potentials for driving nonlinear signals of ferrimagnetic magnon modes in rare-earth-doped garnets.[88] One can also express such magnetization dynamics within the framework of coupled LLG equations similar to Eq. (1) for more than one sublattice. The time-dependent effective magnetic field in Eq. (1) for each sublattice can be calculated as $\mathbf{B}_{\alpha}^{\mathrm{eff}} = -\frac{1}{\gamma_\alpha}\frac{\partial H}{\partial S_\alpha}$, where H is the spin Hamiltonian of the system that describes the microscopy of the interactions[89] leading to the observed nonlinear signals. In the case of $YFeO_3$, H can be expressed as

$$H = -J(\mathbf{S_1}\cdot\mathbf{S_2}) + \mathbf{D}\cdot(\mathbf{S_1}\times\mathbf{S_2}) - \sum_{\substack{i=a,b,c\\ \alpha=1,2}}(K_i S_{\alpha i}^2) - \left[\mathbf{B}_{\mathrm{A}}(t_s,\tau_{\mathrm{delay}}) + \mathbf{B}_{\mathrm{B}}(t_s)\right]\cdot\sum_{\alpha}\gamma_\alpha \mathbf{S}_\alpha, \quad (9)$$

where the first term describes the antiferromagnetic coupling between the neighboring spins $\mathbf{S_1}$ and $\mathbf{S_2}$ that has a negative exchange constant J. The second term describes the Dzyaloshinskii–Moriya interaction with the anti-symmetric exchange parameter $\mathbf{D}$. The third term accounts for the crystalline anisotropy, corresponding to the orthorhombic crystal structure of $YFeO_3$, while the last term is the Zeeman interaction between the spins and the incident THz magnetic fields, thereby accounting for the THz-field-induced nonlinearities in the precession of spins.

In the 2D spectrum corresponding to both the ferromagnetic and the antiferromagnetic modes of $YFeO_3$ [see Fig. 4(f)], a complete set of $\chi^{(3)}$ nonlinear signals have been observed. These signals are: the A-pump-B-probe (PP) signal, the B-pump-A-probe [also called the non-rephasing (NR) peak], the ABB photon echo [also called the rephasing (R) peak], and the AAB photon echo [also called the 2-quantum (2Q) peak]. Additional $\chi^{(2)}$ nonlinear spectral peaks due to second harmonic generation (SHG) and THz rectification (TR) were also identified in the antiferromagnetic mode 2D spectrum.[33] These signals are emitted by the $\chi^{(2)}$ magnetization resulting from sum- and difference-frequency mixing of the magnon coherences generated by each THz pulse.

The excitation of a weak three-magnon bound state has been demonstrated recently in a quasi-one-dimensional antiferromagnet α-$NaMnO_2$ below the antiferromagnetic ordering transition[83] using neutron scattering measurements, see Figs. 4(g)–4(i). This provides an appealing platform for anisotropic triangular antiferromagnets with weak, Ising-like single-ion anisotropy in exploring the dynamics of composite magnon states. There are theoretical proposals of non-collinear magnetic order in magnetic systems that can also harbor a higher-order topological magnon phase and hinge magnon modes,[90] and of three-magnon parametric interaction in a magnetic vortex ground state.[91] The geometry of the magnetization texture is also capable of driving higher-order magnon modes. Using Brillouin light scattering microscopy, it was recently shown that whispering gallery magnons can be generated with unprecedented high wavevectors via nonlinear 3-magnon scattering in a μm-sized magnetic $Ni_{81}Fe_{19}$ discs[92] that are known to inherently exhibit a magnetic vortex structure.[93,94] While the discussed nonlinearities are within the perturbative regime of light-matter interactions, it is possible to go toward the non-perturbative regime, if the THz magnetic fields can be enhanced by using magnetic metamaterials or resonant cavities. Cavity enhancement would allow us to explore the anharmonic couplings between the magnetic modes and the anharmonic magnetic potentials—features that are yet to be explored.

V. CAVITY-ENHANCED NONLINEARITIES

A cavity, of specific interest, is a limited space that can be designed to trap or confine electromagnetic radiation with a desired wavelength (such as, microwave or THz). The confinement simply enhances the spectral amplitude of desired electromagnetic waves

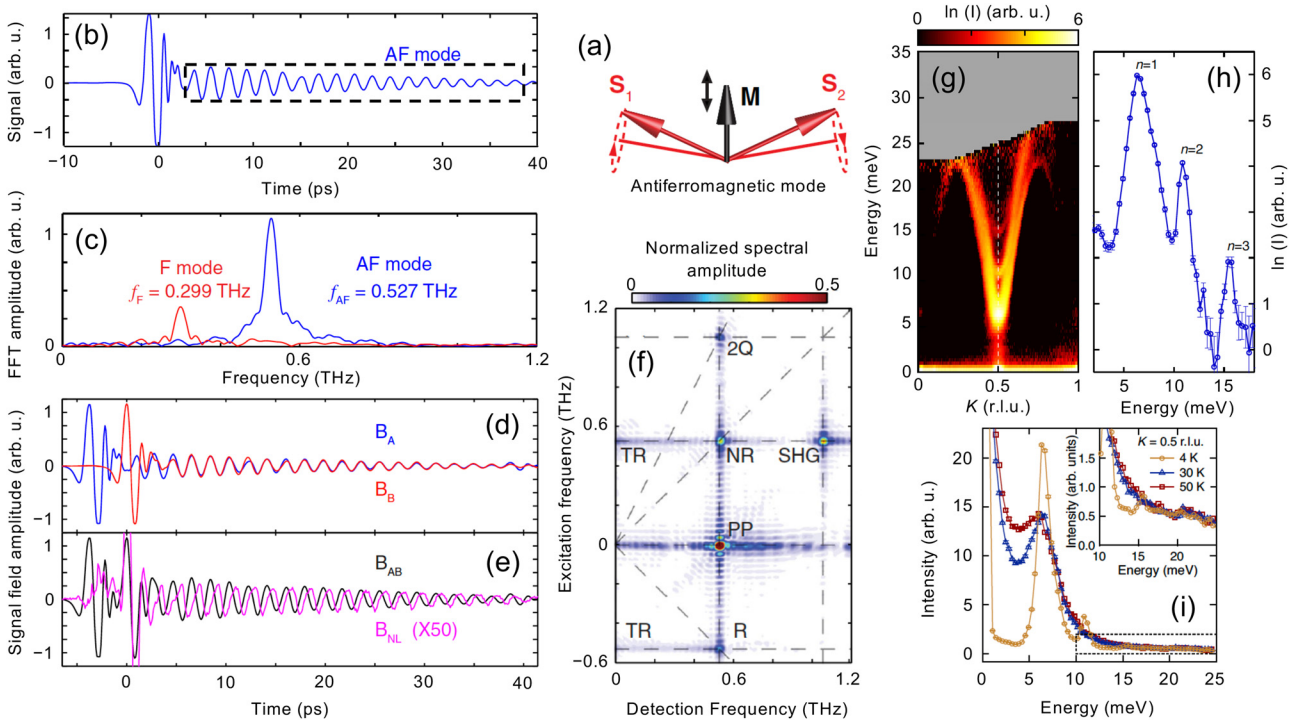

FIG. 4. Higher-order magnon modes. (a) A schematic of the antiferromagnetic mode in $YFeO_3$. (b) THz signal transmitted through the $YFeO_3$ that is followed by free induction decay (FID) signal (marked within the dashed box) corresponding to the antiferromagnetic mode. (c) The spectra showing the antiferromagnetic resonance at 0.53 THz and the ferromagnetic resonance at 0.30 THz. (d) The individual antiferromagnetic magnon signals induced by the two THz pulses. (e) The magnon signal in the presence of both THz pulses when the delay between the two pulses is 3.7 (ps) ($\mathbf{B}_{AB}$, black) and the magnified nonlinear signal ($\mathbf{B}_{NL}$, magenta). (f) The 2D THz spectra for the antiferromagnetic magnon in $YFeO_3$. The $\chi^{(3)}$ spectral peaks include rephasing (R), non-rephasing (NR), pump-probe (PP), and 2-quantum (2Q) peaks, while $\chi^{(2)}$ includes the second harmonic generation (SHG) and THz rectification (TR) peaks. (g) Three magnon excitation branches dispersing along the intrachain direction of quasi-one-dimensional antiferromagnet α-$NaMnO_2$ below the ordering temperature. (h) A slice through the intensity map in (g) centered at the antiferromagnetic zone center, $K = 0.5$. The intensity spectrum clearly shows the three-magnon bound state with $n = 3$ along with the $n = 1$ and $n = 2$ modes. (i) Temperature dependence of the three-magnon bound state at the quasi-1D zone center. Reprinted with permission from Lu *et al.*, Phys. Rev. Lett. **118**, 207204 (2017). Copyright 2017 American Physical Society. Reprinted with permission from Dally *et al.*, Phys. Rev. Lett. **124**, 197203 (2020). Copyright 2020 American Physical Society.[33,83]

within the confined cavity space. It is possible to fill such a cavity with a magnetic material and subsequently tune the interaction of the cavity photons with that of the magnons—the elementary excitations of the magnetic order in the magnetic material.[97,98] As early as 2010, it was predicted that photons in a microwave cavity strongly couple to the dynamics of small ferromagnetic spheres[99] and within the next three years, the observation of strong coupling in the form of an anti-crossing of the collective precession of the magnetization with microwave cavity modes was reported[100] that concomitantly marks the beginning of cavity magnonics. Upon confining magnetic $Y_3Fe_5O_{12}$ (YIG) spheres in a co-planar cavity made of high-purity copper[100] [such as the one shown in Fig. 5(a)] or split-ring resonators[101,102] or 3D microwave cavities,[95,103,104] a strong coupling between the cavity mode and the ferromagnetic Kittel mode have been demonstrated—see the anti-crossing between the two modes in Fig. 5(b). It has also been theoretically reported that by increasing the ratio between the magnet and the cavity sizes, an ultra-strong coupling regime can be entered,[104] while experimental evidence is yet to be shown. A rather direct implication of this is that one can dramatically enhance the electric and magnetic field amplitudes of the electromagnetic radiation of desired wavelengths. Cavity magnonics is a rather emerging field where several cavity-enhanced nonlinearities have been predicted. If the magnetization dynamics are driven into the nonlinear regime, the coupling features, such as the bistability, become dependent on the driving power of the electromagnetic field. It has been theoretically shown that if two magnon modes are trapped in a microwave cavity [similar to the schematic shown in Fig. 5(c)], it is possible to entangle these modes via the nonlinear Kerr effect[105] as the systems are driven far from equilibrium. The nonlinearities of ferromagnets in microwave cavities have been explored in both the classical and quantum regimes in order to assess the resources for quantum information. Strong coupling of microwave cavity photons with multiple magnon modes forms collective bright mode and dark mode that precesses in phase and out of phase, respectively, with the magnetic field.[96] Figure 5(d) shows an illustration of the magnon bright and dark modes. Upon bringing the frequencies of the two magnon modes closer (be setting $\Delta H = 0$), the absorption of the central mode vanishes, giving rise to the dark magnon mode [see Fig. 5(e)]. The two remaining resonances emerge from the hybridization of the bright magnon mode with the cavity photon mode. The formation of bright and dark modes provides evidence of coherent long-range coupling of spatially separated magnets. Such non-local coupling between distant magnets in a cavity

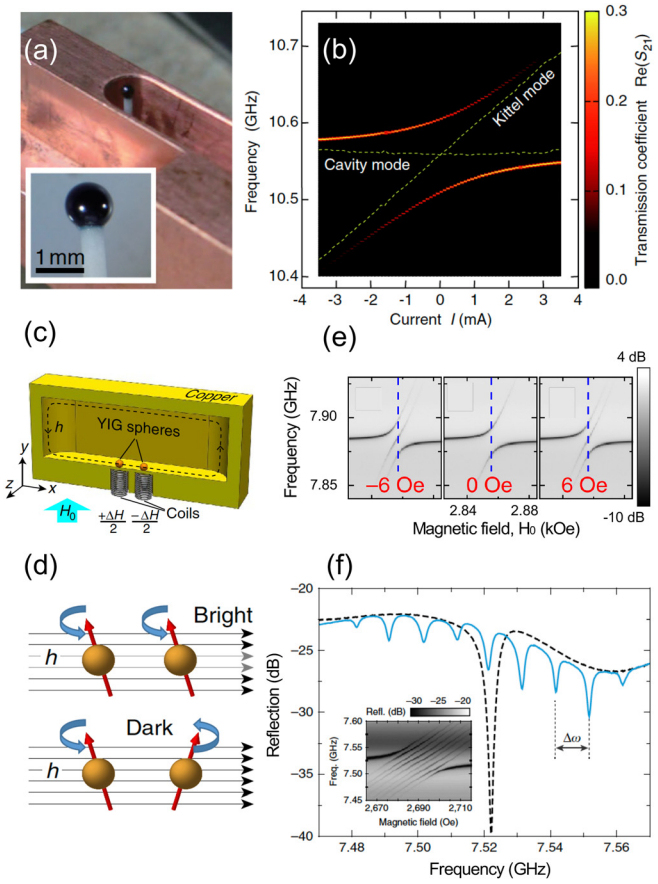

FIG. 5. Magnons in a cavity. (a) A picture of a YIG sphere mounted in a rectangular oxygen-free copper cavity. The inset shows that the sphere is glued to an alumina rod. (b) Transmission amplitude that shows the normal-mode splitting between the Kittel mode and the cavity mode. The amplitude of the transmission through the cavity as a function of the probe microwave frequency and the current through the superconducting coil that generates the magnetic field. (c) A schematic showing two YIG spheres and two small coils in a rectangular copper cavity. H_0 is the external bias magnetic field, ΔH is the magnetic field gradient generated by the small coils, and h magnetic field of the microwave resonance in the cavity. (d) An illustration of the magnon bright and dark modes: The bright mode is coupled to while the dark mode is isolated from the microwave magnetic field. (e) Reflection spectra as a function of bias magnetic field H_0 at a fixed magnetic field gradient $\Delta H = -6, 0$ and 6 Oe, respectively. (f) The reflection spectra of the cavity with eight YIG spheres at a bias field (H_0) of 2.687 Oe (solid blue line) and 0 Oe (dashed black line), respectively. Reprinted with permission from Tabuchi *et al.*, Phys. Rev. Lett. **113**, 083603 (2014). Copyright 2014 American Physical Society.[95] Reprinted with permission from Zhang *et al.*, Nat. Commun. **6**, 8914 (2015). Copyright 2015 Springer Nature Limited.[96]

can, thereby, allow long-range manipulation of spin currents. It is also possible to trap several YIG spheres in the cavity, for example, see the reflection spectrum of eight trapped YIG spheres trapped in Fig. 5(f).

At this stage, while the field is primarily dominated by experiments in the microwave regime, note that such strong cavity magnonics can very well be expanded in the THz regime, where there are neither any theoretical nor experimental reports. The demonstrations of metamaterial-based cavities at THz frequencies are, however, abundant, and thus, it is very natural to expect experimental evidence of cavity-enhanced magnonics and the associated enhanced magnon nonlinearities at THz frequencies in the near future. The demonstration of THz split-ring resonators to enhance the magnetic near-field, normal to the $HoFeO_3$ crystal surface in order to drive the nonlinear magnetization dynamics,[106] provides a promising hint toward THz cavity magnonics.

VI. FUTURE OF MAGNETIZATION NONLINEARITIES

A. Spintronics

Nonlinear ultrafast optical control of spins outstands both the conventional magnetic field-based control and the linear optical control. Nonlinear control of spins inherently benefits from its ever-faster, less dissipative, and easier topologically controlled performance—the future of spin-based devices. Spintronics is an emerging field in the applied research direction, where the efficient manipulation of spin degrees of freedom in quantum systems is one of its most central themes. Nonlinear magnetization control can significantly widen the opportunities of spintronic devices[107] enabling, e.g., the design of magnonic transistors[108] or sensors with increased sensitivity.[109] Direct coupling between the magnetic or electric field of light and the spin system allows efficient control of the spin order in an ultrafast and less-dissipative way, in various magnetic materials. Manipulating magnons with tailored ultrafast light pulses can boost the speed of future magnonic devices.[110] Evidence of ultrafast optically induced transient ferromagnetic state in an antiferromagnet[111] showcases the development toward ultrafast opto-spintronics.[112,113]

B. Nonlinear inertial dynamics

The excitation of nutation resonance modes occurs within the nonlinear regime, lasting for a few hundred femtoseconds after excitation. Even though, such excitation modes have been perceived in ferromagnets with two sublattices, its experimental observation in antiferromagnets is a must due. Moreover, the relaxation time η is not known in such systems. Recent experiments on epitaxial cobalt films also indicate toward a higher harmonics of nutation resonance.[114] To use such THz resonance in ultrafast memory technology, the objective would be to switch the spins at nutation resonance frequencies. As the magnetic moment is not in equilibrium with the angular momentum, this switching mechanism is fundamentally different from the known precessional switching.

C. Nonlinear antiferromagnetic dynamics

Notably, the success in the recent studies on the nonlinear magnetization dynamics in antiferromagnets has pushed the limits for the future of spintronics. This stems from the impact of the antiferromagnets benefiting from various advantages, including robustness against perturbations, no stray fields, ultrafast magnetization dynamics, etc. Moreover, techniques like phononic spin control reveal the possibilities to topologically control the spin order. In addition, technical advancement of nano-designing, such as antenna structures, allows the local optical field enhancement in an integrated way. Besides spintronics, coherent control of spin order can also be applied for the ultrafast read and write of the magnetic memories by adding direct spin torques, paving the way to technological applications like race-track memories, nonvolatile memories, and quantum computing.

D. Nonlinear orbital dynamics

Investigations of nonlinear magnetization dynamics usually consider only spin magnetization, but also the orbital angular momentum that gives rise to magnetic moments. Recent experiments on twisted bilayer graphene revealed a purely orbital magnetism originating from the Berry curvature.[115,116] Although magnetic-field and current-induced switching have been presented, the outreach of ultrafast dynamics of such emerging magnetic order is completely unexplored. A quest in this direction is likely to disclose routes toward manipulating topological states of matter. Given the prominent role of Berry curvature in the emerging field of topological condensed matter, we anticipate groundbreaking discoveries from the exploration of ultrafast nonlinear orbital magnetization dynamics.

VII. CONCLUSION

The tentacles of nonlinearities in the magnetization dynamics have broadened the horizon of future technologies that would use spins for enhancing device functionalities. The advancement in our understandings and controlling these nonlinearities at ultrafast timescales underpins numerous applications ranging from magnonic quantum computation to secure and high speed data transfer and processing. In this Perspective, we have reviewed our current understanding of the outreach of nonlinearities associated with spin precessions from GHz to THz timescales. We also foresee several important and modern aspects of spin dynamics, such as excitation of nutation waves in fully compensated antiferromagnets, modification of magnetization energy landscape using the intrinsic phononic coupling, coherent excitation and control of higher-order magnon modes and cavity quantum electrodynamics with magnons at THz energies. We are hopeful that all these aspects will unfold within the next decade, pushing the importance and realm of nonlinearities in the precession of spins at ultrafast timescales.

ACKNOWLEDGMENTS

J.L. acknowledges the support from Swiss National Science Foundation under Project No. 200021_178825/1. C.-J.Y. acknowledges the financial support from NCCR MUST via No. PSP 1-003448-051. R.M. acknowledges research funding from the Swedish Research Council (VR Grant No. 2019–06313), C.T. acknowledges support from the Harvard University Climate Change Solutions Fund and from the Swiss National Science Foundation under Project No. P2EZP2_191801. S.P. acknowledges the start-up support from DAE through NISER. In addition, S.P. also acknowledges the support from DAE through the project Basic Research in Physical and Multidisciplinary Sciences via No. RIN4001.

AUTHOR DECLARATIONS

Conflict of Interest

The authors do not have any conflicts of interest to declare.

DATA AVAILABILITY

The data that support the findings of this study are available from the corresponding authors upon reasonable request.

REFERENCES

[1]M. Getzlaff, *Fundamentals of Magnetism* (Springer, 2008).
[2]E. Olive, Y. Lansac, M. Meyer, M. Hayoun, and J.-E. Wegrowe, J. Appl. Phys. **117**, 213904 (2015).
[3]J. F. Dobson, Phys. Rev. Lett. **73**, 2244 (1994).
[4]W. Kohn, Phys. Rev. **123**, 1242 (1961).
[5]T. Tél and M. Gruiz, *Chaotic Dynamics: An Introduction Based on Classical Mechanics* (Cambridge University Press, 2006).
[6]B. Hillebrands and K. Ounadjela, *Spin Dynamics in Confined Magnetic Structures I* (Springer Science & Business Media, 2002).
[7]Y. Tserkovnyak, A. Brataas, G. E. W. Bauer, and B. I. Halperin, Rev. Mod. Phys. **77**, 1375 (2005).
[8]C. H. Back, D. Weller, J. Heidmann, D. Mauri, D. Guarisco, E. L. Garwin, and H. C. Siegmann, Phys. Rev. Lett. **81**, 3251 (1998).
[9]I. Tudosa, C. Stamm, A. Kashuba, F. King, H. Siegmann, J. Stöhr, G. Ju, B. Lu, and D. Weller, Nature **428**, 831 (2004).
[10]A. Kirilyuk, A. V. Kimel, and T. Rasing, Rev. Mod. Phys. **82**, 2731 (2010).
[11]E. Beaurepaire, J.-C. Merle, A. Daunois, and J.-Y. Bigot, Phys. Rev. Lett. **76**, 4250 (1996).
[12]W. Zhang, P. Maldonado, Z. Jin, T. S. Seifert, J. Arabski, G. Schmerber, E. Beaurepaire, M. Bonn, T. Kampfrath, P. M. Oppeneer, and D. Turchinovich, Nat. Commun. **11**, 4247 (2020).
[13]F. Siegrist, J. A. Gessner, M. Ossiander, C. Denker, Y.-P. Chang, M. C. Schröder, A. Guggenmos, Y. Cui, J. Walowski, U. Martens, J. K. Dewhurst, U. Kleineberg, M. Münzenberg, S. Sharma, and M. Schultze, Nature **571**, 240 (2019).
[14]S. Baierl, M. Hohenleutner, T. Kampfrath, A. K. Zvezdin, A. V. Kimel, R. Huber, and R. V. Mikhaylovskiy, Nat. Photonics **10**, 715 (2016).
[15]S. Baierl, J. H. Mentink, M. Hohenleutner, L. Braun, T.-M. Do, C. Lange, A. Sell, M. Fiebig, G. Woltersdorf, T. Kampfrath, and R. Huber, Phys. Rev. Lett. **117**, 197201 (2016).
[16]R. Mikhaylovskiy, E. Hendry, A. Secchi, J. H. Mentink, M. Eckstein, A. Wu, R. Pisarev, V. Kruglyak, M. Katsnelson, T. Rasing *et al.*, Nat. Commun. **6**, 8190 (2015).
[17]C.-H. Lambert, S. Mangin, B. C. S. Varaprasad, Y. Takahashi, M. Hehn, M. Cinchetti, G. Malinowski, K. Hono, Y. Fainman, M. Aeschlimann *et al.*, Science **345**, 1337 (2014).
[18]S. O. Mariager, F. Pressacco, G. Ingold, A. Caviezel, E. Möhr-Vorobeva, P. Beaud, S. Johnson, C. Milne, E. Mancini, S. Moyerman *et al.*, Phys. Rev. Lett. **108**, 087201 (2012).
[19]C. D. Stanciu, F. Hansteen, A. V. Kimel, A. Kirilyuk, A. Tsukamoto, A. Itoh, and T. Rasing, Phys. Rev. Lett. **99**, 047601 (2007).
[20]A. V. Kimel, A. Kirilyuk, F. Hansteen, R. V. Pisarev, and T. Rasing, J. Phys.: Condens. Matter **19**, 043201 (2007).
[21]M. Berritta, R. Mondal, K. Carva, and P. M. Oppeneer, Phys. Rev. Lett. **117**, 137203 (2016).
[22]M. Nakajima, A. Namai, S. Ohkoshi, and T. Suemoto, Opt. Express **18**, 18260 (2010).
[23]K. Yamaguchi, M. Nakajima, and T. Suemoto, Phys. Rev. Lett. **105**, 237201 (2010).
[24]S. Bonetti, M. C. Hoffmann, M.-J. Sher, Z. Chen, S.-H. Yang, M. G. Samant, S. S. P. Parkin, and H. A. Dürr, Phys. Rev. Lett. **117**, 087205 (2016).
[25]T. Kurihara, H. Watanabe, M. Nakajima, S. Karube, K. Oto, Y. Otani, and T. Suemoto, Phys. Rev. Lett. **120**, 107202 (2018).
[26]R. C. Hilborn, *Chaos and Nonlinear Dynamics* (Oxford University Press, 2000).
[27]Note that the subscripts A and B refer to different perturbations of the magnetic order. The subscripts do not refer to different magnetic sublattices. In case of a multi-sublattice magnet, Eqs. (2) and (3) apply to each sublattice individually. An additional subscript for the sublattice is omitted.
[28]M. Hudl, M. d'Aquino, M. Pancaldi, S.-H. Yang, M. G. Samant, S. S. P. Parkin, H. A. Dürr, C. Serpico, M. C. Hoffmann, and S. Bonetti, Phys. Rev. Lett. **123**, 197204 (2019).
[29]W. Kuehn, K. Reimann, M. Woerner, T. Elsaesser, and R. Hey, J. Phys. Chem. B **115**, 5448 (2011).
[30]M. Woerner, W. Kuehn, P. Bowlan, K. Reimann, and T. Elsaesser, New J. Phys. **15**, 025039 (2013).

[31]G. Folpini, D. Morrill, C. Somma, K. Reimann, M. Woerner, T. Elsaesser, and K. Biermann, Phys. Rev. B **92**, 085306 (2015).
[32]C. Somma, G. Folpini, K. Reimann, M. Woerner, and T. Elsaesser, Phys. Rev. Lett. **116**, 177401 (2016).
[33]J. Lu, X. Li, H. Y. Hwang, B. K. Ofori-Okai, T. Kurihara, T. Suemoto, and K. A. Nelson, Phys. Rev. Lett. **118**, 207204 (2017).
[34]G. Folpini, K. Reimann, M. Woerner, T. Elsaesser, J. Hoja, and A. Tkatchenko, Phys. Rev. Lett. **119**, 097404 (2017).
[35]Y. Wan and N. P. Armitage, Phys. Rev. Lett. **122**, 257401 (2019).
[36]K. Reimann, M. Woerner, and T. Elsaesser, J. Chem. Phys. **154**, 120901 (2021).
[37]A. V. Kimel, A. Kirilyuk, P. A. Usachev, R. V. Pisarev, A. M. Balbashov, and T. Rasing, Nature **435**, 655 (2005).
[38]A. M. Kalashnikova, A. V. Kimel, R. V. Pisarev, V. N. Gridnev, A. Kirilyuk, and T. Rasing, Phys. Rev. Lett. **99**, 167205 (2007).
[39]T. Satoh, S.-J. Cho, R. Iida, T. Shimura, K. Kuroda, H. Ueda, Y. Ueda, B. A. Ivanov, F. Nori, and M. Fiebig, Phys. Rev. Lett. **105**, 077402 (2010).
[40]C. Tzschaschel, K. Otani, R. Iida, T. Shimura, H. Ueda, S. Günther, M. Fiebig, and T. Satoh, Phys. Rev. B **95**, 174407 (2017).
[41]C. Tzschaschel, T. Satoh, and M. Fiebig, Nat. Commun. **11**, 6142 (2020).
[42]Y. Li, V. V. Naletov, O. Klein, J. L. Prieto, M. Munoz, V. Cros, P. Bortolotti, A. Anane, C. Serpico, and G. de Loubens, Phys. Rev. X **9**, 041036 (2019).
[43]C. Tzschaschel, T. Satoh, and M. Fiebig, Nat. Commun. **10**, 3995 (2019).
[44]M. Białek, T. Ito, H. Rønnow, and J.-P. Ansermet, Phys. Rev. B **99**, 064429 (2019).
[45]M. Białek, J. Zhang, H. Yu, and J.-P. Ansermet, Phys. Rev. Appl. **15**, 044018 (2021).
[46]R. Mondal, A. Donges, U. Ritzmann, P. M. Oppeneer, and U. Nowak, Phys. Rev. B **100**, 060409(R) (2019).
[47]R. Mondal, A. Donges, and U. Nowak, Phys. Rev. Res. **3**, 023116 (2021).
[48]H. Suhl, IEEE Trans. Magn. **34**, 1834 (1998).
[49]M.-C. Ciornei, J. M. Rubí, and J.-E. Wegrowe, Phys. Rev. B **83**, 020410 (2011).
[50]D. Böttcher and J. Henk, Phys. Rev. B **86**, 020404 (2012).
[51]J.-E. Wegrowe and M.-C. Ciornei, Am. J. Phys. **80**, 607 (2012).
[52]M. Fähnle, D. Steiauf, and C. Illg, Phys. Rev. B **84**, 172403 (2011).
[53]R. Mondal, M. Berritta, A. K. Nandy, and P. M. Oppeneer, Phys. Rev. B **96**, 024425 (2017).
[54]R. Mondal, M. Berritta, and P. M. Oppeneer, Phys. Rev. B **98**, 214429 (2018).
[55]K. Neeraj, N. Awari, S. Kovalev, D. Polley, N. Zhou Hagström, S. S. P. K. Arekapudi, A. Semisalova, K. Lenz, B. Green, J.-C. Deinert, I. Ilyakov, M. Chen, M. Bawatna, V. Scalera, M. d'Aquino, C. Serpico, O. Hellwig, J.-E. Wegrowe, M. Gensch, and S. Bonetti, Nat. Phys. **17**, 245 (2021).
[56]S. Bhattacharjee, L. Nordström, and J. Fransson, Phys. Rev. Lett. **108**, 057204 (2012).
[57]S. Giordano and P.-M. Déjardin, Phys. Rev. B **102**, 214406 (2020).
[58]S. V. Titov, W. T. Coffey, Y. P. Kalmykov, M. Zarifakis, and A. S. Titov, Phys. Rev. B **103**, 144433 (2021).
[59]S. V. Titov, W. T. Coffey, Y. P. Kalmykov, and M. Zarifakis, Phys. Rev. B **103**, 214444 (2021).
[60]R. Mondal, M. Berritta, and P. M. Oppeneer, J. Phys.: Condens. Matter **30**, 265801 (2018).
[61]E. Olive, Y. Lansac, and J.-E. Wegrowe, Appl. Phys. Lett. **100**, 192407 (2012).
[62]M. Cherkasskii, M. Farle, and A. Semisalova, Phys. Rev. B **102**, 184432 (2020).
[63]M. Cherkasskii, M. Farle, and A. Semisalova, Phys. Rev. B **103**, 174435 (2021).
[64]R. Mondal, J. Phys.: Condens. Matter **33**, 275804 (2021).
[65]R. Mondal, S. Großenbach, L. Rózsa, and U. Nowak, Phys. Rev. B **103**, 104404 (2021).
[66]R. Mondal and P. M. Oppeneer, Phys. Rev. B **104**, 104405 (2021).
[67]R. Mondal and A. Kamra, Phys. Rev. B **104**, 214426 (2021).
[68]A. V. Kimel, B. A. Ivanov, R. V. Pisarev, P. A. Usachev, A. Kirilyuk, and T. Rasing, Nat. Phys. **5**, 727 (2009).
[69]R. Mondal, M. Berritta, and P. M. Oppeneer, Phys. Rev. B **94**, 144419 (2016).
[70]T. G. H. Blank, K. A. Grishunin, E. A. Mashkovich, M. V. Logunov, A. K. Zvezdin, and A. V. Kimel, Phys. Rev. Lett. **127**, 037203 (2021).
[71]T. F. Nova, A. Cartella, A. Cantaluppi, M. Först, D. Bossini, R. V. Mikhaylovskiy, A. V. Kimel, R. Merlin, and A. Cavalleri, Nat. Phys. **13**, 132 (2017).
[72]D. Afanasiev, J. R. Hortensius, B. A. Ivanov, A. Sasani, E. Bousquet, Y. M. Blanter, R. V. Mikhaylovskiy, A. V. Kimel, and A. D. Caviglia, Nat. Mater. **20**, 607 (2021).
[73]A. S. Disa, M. Fechner, T. F. Nova, B. Liu, M. Först, D. Prabhakaran, P. G. Radaelli, and A. Cavalleri, Nat. Phys. **16**, 937 (2020).
[74]A. K. Zvezdin and V. M. Matveev, Sov. Phys. JETP **77**, 1076 (1979), available at http://inis.iaea.org/search/search.aspx?orig_q=RN:11506653.
[75]D. M. Juraschek, P. Narang, and N. A. Spaldin, Phys. Rev. Res. **2**, 043035 (2020).
[76]M. Fechner, A. Sukhov, L. Chotorlishvili, C. Kenel, J. Berakdar, and N. A. Spaldin, Phys. Rev. Mater. **2**, 064401 (2018).
[77]A. Stupakiewicz, C. S. Davies, K. Szerenos, D. Afanasiev, K. S. Rabinovich, A. V. Boris, A. Caviglia, A. V. Kimel, and A. Kirilyuk, Nat. Phys. **17**, 489 (2021).
[78]A. Melnikov, I. Radu, U. Bovensiepen, O. Krupin, K. Starke, E. Matthias, and M. Wolf, Phys. Rev. Lett. **91**, 227403 (2003).
[79]R. Mankowsky, M. Först, and A. Cavalleri, Rep. Prog. Phys. **79**, 064503 (2016).
[80]S. Schlauderer, C. Lange, S. Baierl, T. Ebnet, C. P. Schmid, D. C. Valovcin, A. K. Zvezdin, A. V. Kimel, R. V. Mikhaylovskiy, and R. Huber, Nature **569**, 383 (2019).
[81]A. Stupakiewicz, K. Szerenos, D. Afanasiev, A. Kirilyuk, and A. V. Kimel, Nature **542**, 71 (2017).
[82]S. F. Maehrlein, I. Radu, P. Maldonado, A. Paarmann, M. Gensch, A. M. Kalashnikova, R. V. Pisarev, M. Wolf, P. M. Oppeneer, J. Barker, and T. Kampfrath, Sci. Adv. **4**, eaar5164 (2018).
[83]R. L. Dally, A. J. R. Heng, A. Keselman, M. M. Bordelon, M. B. Stone, L. Balents, and S. D. Wilson, Phys. Rev. Lett. **124**, 197203 (2020).
[84]T. Kampfrath, A. Sell, G. Klatt, A. Pashkin, S. Mährlein, T. Dekorsy, M. Wolf, M. Fiebig, A. Leitenstorfer, and R. Huber, Nat. Photonics **5**, 31 (2011).
[85]S. Pal, N. Strkalj, C.-J. Yang, M. C. Weber, M. Trassin, M. Woerner, and M. Fiebig, Phys. Rev. X **11**, 021023 (2021).
[86]S. Markmann, M. Franckié, S. Pal, D. Stark, M. Beck, M. Fiebig, G. Scalari, and J. Faist, Nanophotonics **10**, 171 (2020).
[87]J. Raab, C. Lange, J. L. Boland, I. Laepple, M. Furthmeier, E. Dardanis, N. Dessmann, L. Li, E. H. Linfield, A. G. Davies, M. S. Vitiello, and R. Huber, Opt. Express **27**, 2248 (2019).
[88]S. Pal, C. Tzschaschel, A. Bortis, T. Satoh, and M. Fiebig, in *Conference on Lasers and Electro-Optics* (Optical Society of America, 2019) FM3D.3.
[89]G. Herrmann, J. Phys. Chem. Solids **24**, 597 (1963).
[90]M. J. Park, S. Lee, and Y. B. Kim, Phys. Rev. B **104**, L060401 (2021).
[91]R. Verba, L. Körber, K. Schultheiss, H. Schultheiss, V. Tiberkevich, and A. Slavin, Phys. Rev. B **103**, 014413 (2021).
[92]K. Schultheiss, R. Verba, F. Wehrmann, K. Wagner, L. Körber, T. Hula, T. Hache, A. Kákay, A. A. Awad, V. Tiberkevich, A. N. Slavin, J. Fassbender, and H. Schultheiss, Phys. Rev. Lett. **122**, 097202 (2019).
[93]T. Shinjo, T. Okuno, R. Hassdorf, K. Shigeto, and T. Ono, Science **289**, 930 (2000).
[94]K. Y. Guslienko, A. N. Slavin, V. Tiberkevich, and S.-K. Kim, Phys. Rev. Lett. **101**, 247203 (2008).
[95]Y. Tabuchi, S. Ishino, T. Ishikawa, R. Yamazaki, K. Usami, and Y. Nakamura, Phys. Rev. Lett. **113**, 083603 (2014).
[96]X. Zhang, C.-L. Zou, N. Zhu, F. Marquardt, L. Jiang, and H. X. Tang, Nat. Commun. **6**, 8914 (2015).
[97]M. Elyasi, Y. M. Blanter, and G. E. Bauer, Phys. Rev. B **101**, 054402 (2020).
[98]B. Z. Rameshti, S. V. Kusminskiy, J. A. Haigh, K. Usami, D. Lachance-Quirion, Y. Nakamura, C.-M. Hu, H. X. Tang, G. E. Bauer, and Y. M. Blanter, arXiv:2106.09312 [cond-mat.mes-hall] (2021).
[99]Ö. O. Soykal and M. E. Flatté, Phys. Rev. Lett. **104**, 077202 (2010).
[100]H. Huebl, C. W. Zollitsch, J. Lotze, F. Hocke, M. Greifenstein, A. Marx, R. Gross, and S. T. B. Goennenwein, Phys. Rev. Lett. **111**, 127003 (2013).
[101]B. Bhoi, T. Cliff, I. S. Maksymov, M. Kostylev, R. Aiyar, N. Venkataramani, S. Prasad, and R. L. Stamps, J. Appl. Phys. **116**, 243906 (2014).
[102]G. B. G. Stenning, G. J. Bowden, L. C. Maple, S. A. Gregory, A. Sposito, R. W. Eason, N. I. Zheludev, and P. A. J. de Groot, Opt. Express **21**, 1456 (2013).

[103]M. Goryachev, W. G. Farr, D. L. Creedon, Y. Fan, M. Kostylev, and M. E. Tobar, Phys. Rev. Appl. **2**, 054002 (2014).
[104]X. Zhang, C.-L. Zou, L. Jiang, and H. X. Tang, Phys. Rev. Lett. **113**, 156401 (2014).
[105]Y.-P. Wang, G.-Q. Zhang, D. Zhang, X.-Q. Luo, W. Xiong, S.-P. Wang, T.-F. Li, C.-M. Hu, and J. Q. You, Phys. Rev. B **94**, 224410 (2016).
[106]Y. Mukai, H. Hirori, T. Yamamoto, H. Kageyama, and K. Tanaka, New J. Phys. **18**, 013045 (2016).
[107]A. Hoffmann and S. D. Bader, Phys. Rev. Appl. **4**, 047001 (2015).
[108]A. V. Chumak, A. A. Serga, and B. Hillebrands, Nat. Commun. **5**, 4700 (2014).
[109]M. P. Nikitin, A. V. Orlov, I. L. Sokolov, A. A. Minakov, P. I. Nikitin, J. Ding, S. D. Bader, E. A. Rozhkova, and V. Novosad, Nanoscale **10**, 11642 (2018).
[110]N. Singh, P. Elliott, J. K. Dewhurst, and S. Sharma, Phys. Rev. B **103**, 134402 (2021).
[111]E. Golias, I. Kumberg, I. Gelen, S. Thakur, J. Gördes, R. Hosseinifar, Q. Guillet, J. K. Dewhurst, S. Sharma, C. Schüßler-Langeheine, N. Pontius, and W. Kuch, Phys. Rev. Lett. **126**, 107202 (2021).
[112]V. Baltz, A. Manchon, M. Tsoi, T. Moriyama, T. Ono, and Y. Tserkovnyak, Rev. Mod. Phys. **90**, 015005 (2018).
[113]P. Němec, M. Fiebig, T. Kampfrath, and A. V. Kimel, Nat. Phys. **14**, 229 (2018).
[114]V. Unikandanunni, R. Medapalli, M. Asa, E. Albisetti, D. Petti, R. Bertacco, E. E. Fullerton, and S. Bonetti, arXiv:2109.03076 [cond-mat.mes-hall] (2021).
[115]A. L. Sharpe, E. J. Fox, A. W. Barnard, J. Finney, K. Watanabe, T. Taniguchi, M. A. Kastner, and D. Goldhaber-Gordon, Science **365**, 605 (2019).
[116]M. Serlin, C. L. Tschirhart, H. Polshyn, Y. Zhang, J. Zhu, K. Watanabe, T. Taniguchi, L. Balents, and A. F. Young, Science **367**, 900 (2020).